polymers

MDPI

Article

Study of a Novel Electrochromic Device with Crystalline WO_3 and Gel Electrolyte

Wanyu Chen [1], Guixia Zhang [1], Lili Wu [1], Siyuan Liu [1], Meng Cao [1], Ying Yang [1] and Yong Peng [2,*]

[1] School of Materials Science and Engineering, Wuhan University of Technology, Wuhan 430070, China; chenwanyu@whut.edu.cn (W.C.); zhang94670@whut.edu.cn (G.Z.); polym_wl@whut.edu.cn (L.W.); liusiyuan_ysl@whut.edu.cn (S.L.); caomeng19970705@163.com (M.C.); yingyang2006@163.com (Y.Y.)

[2] State Key Laboratory of Advanced Technology for Materials Synthesis and Processing, Wuhan University of Technology, Wuhan 430070, China

* Correspondence: yongpeng@whut.edu.cn

Abstract: Most ECDs are coated with an electrochromic material on the transparent conductive oxide (TCO) substrate. A novel electrochromic device (ECD), having a variable optical performance, was prepared by using tungsten foil as a substrate in this study. It was found that the WO_3 discoloration layer, having a monoclinic phase crystalline structure made of 600 °C calcined, had optimum charge transmission performance with PADA gel polymer electrolyte. Ionic conductivity of PADA gel polymer electrolyte was 2.3×10^{-3} S cm^{-1} at −20 °C, and it was possible to help Li^+ to implement embedding and extraction from WO_3 even in low-temperature conditions. The colored time (t_c) and the bleached time (t_b) of the electrochromic device were 15 s and 26 s, and it showed yellowish-brown in the colored state and navy blue in the bleached state. The ECD (WO_3-600) exhibited good cycle stability reach at least 150 times.

Keywords: electrochromic device; crystalline tungsten oxide; ionically cross-linked gel; conductivity

Citation: Chen, W.; Zhang, G.; Wu, L.; Liu, S.; Cao, M.; Yang, Y.; Peng, Y. Study of a Novel Electrochromic Device with Crystalline WO_3 and Gel Electrolyte. *Polymers* **2022**, *14*, 1430. https://doi.org/10.3390/polym14071430

Academic Editors: Chi-Jung Chang and Mohammad Afsar Uddin

Received: 11 March 2022
Accepted: 29 March 2022
Published: 31 March 2022

1. Introduction

Electrochromism refers to a reversible change in the electronic structure and optical properties (reflectance, transmittance or absorption) of electrochromic materials under an applied voltage [1–4]. Electrochromic phenomena have a wide range of applications in the fields of smart windows, displays, anti-glare rearview mirrors, smart thermal control and camouflage, etc., [5–8]. WO_3, an electrochromic layer material, has been widely used in inorganic electrochromic and other related technical fields because of its advantages, such as high-color contrast, low manufacturing cost, non-toxicity, and stability under acidic and oxidizing conditions [9–17].

Normally, WO_3 layers are prepared on top of transparent conductive oxide (TCO) via hydrothermal method, sol–gel progress, sputtering, etc. [18–21], and ECD mostly consists of TCO/cathode electrode/electrolyte/anode electrode. However, TCO is not cheap, and the preparation process of WO_3 is relatively complex. For example, Pooyodying, et al., focused on the coating of WO_3 on PET/ITO substrates [22]. In addition, there are different phases of WO_3, such as orthorhombic, monoclinic (m-WO_3), triclinic, tetragonal (t-WO_3), hexagonal (h-WO_3), etc., [23–27]. The structure of WO_3 prepared by these synthesis methods is mostly orthorhombic and monoclinic phase [23,28,29]. In this paper, a novel method was the preparation of the WO_3 layer on tungsten foil via direct oxidization at high temperatures. The WO_3 had a porous structure and three crystal phases after calcining, and its new performance application was given. The porous crystalline WO_3 film had high porosity, specific surface area, better stability, and higher strength and corrosion resistance [30], which affected charge carriers transporting during working. Three different crystals of hexagonal, tetragonal and monoclinic phase of WO_3 on EC properties were investigated.

As the ion transport layer, the electrolyte is located in the middle layer of the electrochromic device, and is the conductive medium between the electrodes. Therefore, it is very important that the electrolyte has good performance in terms of electrical conductivity and electrochemical stability. In addition, the electrolyte used needs to have a high transmittance to effectively avoid influencing the color modulation of the electrochromic material. Gel polymer electrolyte combines the advantages of liquid electrolyte and solid electrolyte with good flexibility, high ionic conductivity, and a wide electrochemical stability window, which has made it widely studied, such as when PVDF-co-HFP/[Li][TFSI] gel electrolytes were designed for flexible WO_3-based ECDs [31].

In this research, the prepared PADA gel electrolyte had a high-transmittance, high-ion conductivity and a wide electrochemical stability window. The compatibility of the electrochromic layer with the ion transport layer also affected the performance of the electrochromic device. An electrochromic device composed of copper-conductive adhesive/tungsten oxide foil/gel electrolyte/nickel foil/transparent PET film was assembled. The three crystal phases of the tungsten oxide and the PADA gel electrolyte were assembled into an electrochromic device (referred to as ECD (WO_3-400), ECD (WO_3-500), ECD (WO_3-600)) by multi-sandwiching, and its optical performance and cycle stability was studied.

2. Experimental Section

2.1. Materials

N,N-dimethylformamide (DMF, AR) was purchased from Sinopharm Chemical Reagent Co., Ltd. (Shanghai, China). Lithium perchlorate ($LiClO_4$, anhydrous, 99.9%), propylene carbonate (PC, anhydrous, 99.7%), acrylic acid (AA, purity > 99%), acrylamide (AAm, 99%) and 2-diethylaminoethyl methacrylate (DEAM, 99%) were purchased from Aladdin (Shanghai, China). Azobisisobutyronitrile (AIBN, AR) was provided by Sigma–Aldrich. (Shanghai, China). Tungsten (99.99%) was purchased from Xinyi Metal Co., Ltd. (Xingtai, China).

2.2. Synthesis of PADA Gel Polymer

The specific synthesis process was as follows [32]: firstly, 0.5032 g $LiClO_4$ was added into a mixed solution of 2.5 mL of propylene carbonate (PC) and 2.5 mL of N,N-dimethyl formamide (DMF), and stirred until the solution became transparent and clear. Secondly, 0.5 mL of diethylaminoethyl methacrylate (DEAM) and 0.5 mL of acrylic acid (AA) were added as ion associations into the mixed solution. Thirdly, 250 mg of comonomer acrylamide (AAm) was added. Fourthly, 1.25 mg of AIBN was added to induce initiation. Fifthly, by stirring at room temperature for 2 h, an homogeneous solution was obtained. Finally, the oxygen-free purity mixture was put into a clean and sealed glass container and heated at 80 °C for 8 h to form PADA gel electrolyte. Table 1 shows the proportion composition of different PADA gels.

Table 1. Proportion composition of PADA gel electrolyte.

	PADA-a	PADA-b	PADA-c
PC (mL)	2.5	2.5	2.5
DMF (mL)	2.5	2.5	2.5
$LiClO_4$ (g)	0.5032	0.5032	0.5032
DEAM (mL)	0.2	0.5	0.8
AA (mL)	0.8	0.5	0.2
AAm (mg)	250	250	250
AIBN (mg)	1.25	1.25	1.25

2.3. Assembly of PECD

A clean tungsten foil was put in a crucible and was then transferred to a KSL-1100X box furnace for calcining. The oxidizing temperatures were set to a fixed value (such as 400 °C

or 500 °C or 600 °C) for 3 h. Then, oxidized tungsten was prepared for device assembling. As shown in Figure 1, the electrochromic device was assembled to be a sandwich structure of copper-conductive adhesive/tungsten oxide foil/gel electrolyte/nickel foil/transparent PET film.

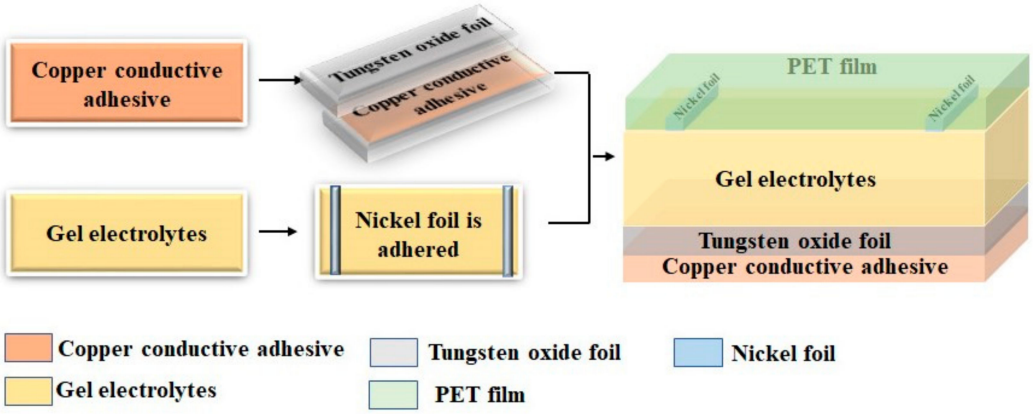

Figure 1. Assembly of PECD.

2.4. Characterization

The phase state tungsten of the tungsten oxide was analyzed by X-ray diffraction (XRD, D8 Advance X, Bruker, AXS, Karlsruhe, Germany), using Cu-Kα as the target, with a scanning range of 20–90° and a scanning speed of 10 mv/s.

The microstructure, morphology and atomic composition of the WO_3 were characterized by using a field emission scanning electron microscope with an X-Max N80 spectrometer (FE-SEM, JSM-7500F, JEOL, Tokyo, Japan).

Optical reflectivity of the electrochromic device was measured by using an ultraviolet, visible, near-infrared spectrophotometer (Lambda 750S, PerkinElmer, Waltham, MA, USA) with a wavelength range of 400–700 nm.

An electrochemical workstation (SP300, Bio-Logic, Seyssinet-Pariset, France) was used to measure the electrochemical impedance spectroscopy (EIS) behavior of the PADA gel electrolyte at a frequency of 0.1 Hz–1 MHz and a temperature of −20–80 °C. The structure of the test device was Pt/PADA gel electrolyte/Pt. The equivalent circuit diagram of the gel electrolyte was obtained by fitting Zview software.

3. Results and Discussion

3.1. Optical Properties of Electrochromic Devices

Figure 2a,b show the colored state and the bleached state of ECD (WO_3-600), respectively. ECD (WO_3-600) shows yellowish-brown in the colored state and navy blue in the bleached state. The optical modulation amplitude is defined as the reflectivity difference between the colored state and the bleached state. Figure 2c–e show that the reflectivity of the colored state ECD (WO_3-600) and the bleached state of ECD (WO_3-600) under a voltage of ±3 V at 700 nm are 16.59% and 12.49%, respectively; the optical modulation amplitude is 4.1%. Compared with ECD (WO_3-400) and ECD (WO_3-500), ECD (WO_3-600) has a larger optical modulation amplitude, which indicates that ECD (WO_3-600) is more suitable as an electrochromic device.

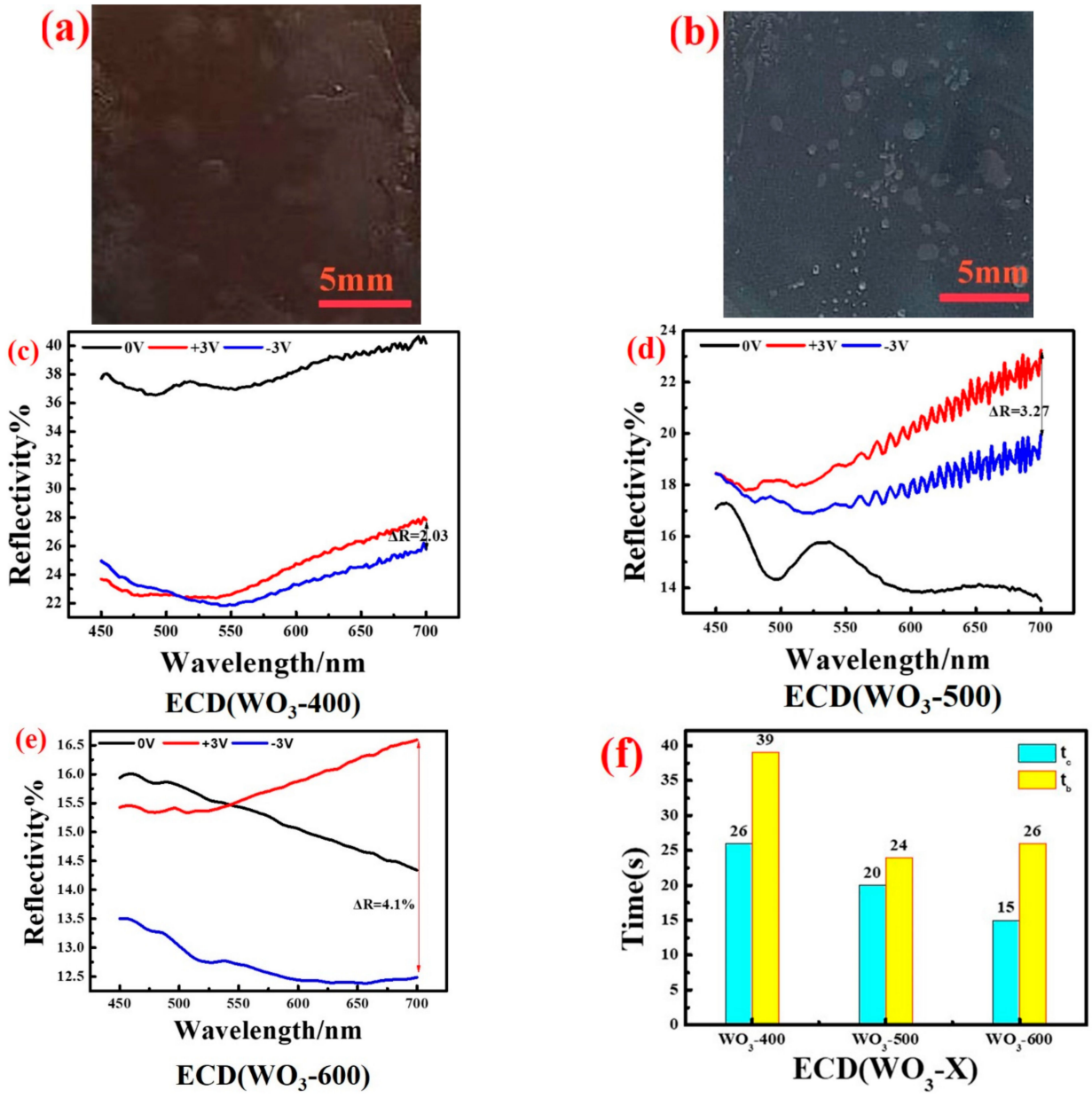

Figure 2. (**a**) Photo of the colored state of the electrochromic device; (**b**) Photo of the bleached state of the electrochromic device; (**c**) ECD reflectance spectrum of WO_3-400 under different voltage conditions; (**d**) ECD reflectance spectrum of WO_3-500 under different voltage conditions; (**e**) ECD reflectance spectrum of WO_3-600 under different voltage conditions; (**f**) Coloring and bleaching time of ECD (WO_3-X).

The response time of an electrochromic device is defined as the time required for the electrochromic device to complete 90% of the maximum optical modulation amplitude. Figure 2f shows the coloring and bleaching time of different electrochromic devices. Compared to ECD (WO_3-400) and ECD (WO_3-500), the coloring time of ECD (WO_3-600), whose color switch change rate is t_c/t_b = 15/26, is shorter. The electrochromic device has a large optical modulation amplitude and color change speed: these are associated with the transparency and ion conductivity of the gel electrolyte.

Based on the transmittance test of the PADA gel electrolyte, synthesized with different DEAM and AA volume ratios in the wavelength range of 400–800 nm, Figure 3 shows that the transparency of the PADA-b gel electrolyte is higher than that of PADA-a and PADA-c. This may be the reason why the volume ratio of the AA and DEAM is 1:1, the

compatibility between the polymer and the solvent is optimal—forming a compatible gel system which exhibits high transparency [32]—and its optical transmittance exceeds 98% in the range of 610–800 nm, and reaches 99.88% at 800 nm. However, the transmittance of some organic polymer gel electrolytes such as PEO and PI is within 80–90% [33–38]. The high transmittance of the gel electrolyte is better used in electrochromic devices; the difference in transmittance or reflectivity between the colored state and the bleached state of the electrochromic device can be clearly observed.

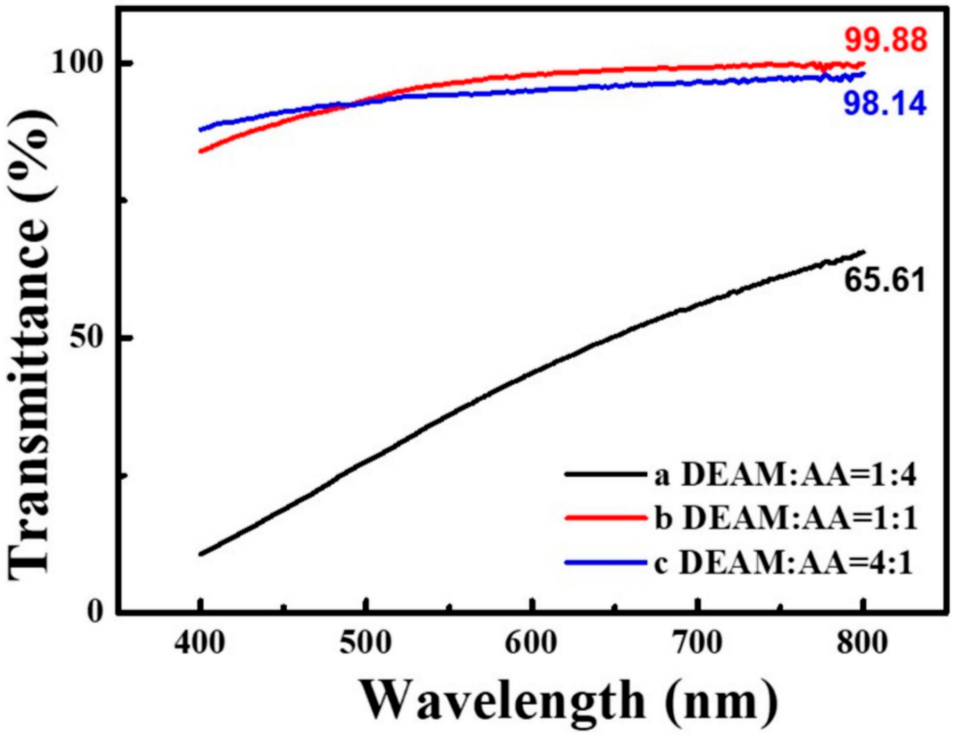

Figure 3. Transmittance spectra of PADA gel electrolytes with different volume ratios of DEAM and AA at wavelengths of 400–800 nm.

We conducted electrical impedance testing of the synthesized PADA-a, PADA-b, PADA-c and liquid electrolyte to analyze their ionic conductivity. Ionic conductivity plays an important role in determining the efficiency of ion transport in the electrolyte, which greatly affects the performance of electrochromic devices. As the ion-transport efficiency of the electrolyte has a great influence on the response time of the coloring and fading process of the electrochromic device, it is also one of the major indicators of the performance of the ECD.

Figure 4a shows the AC impedance spectra of different PADA gel electrolytes and liquid electrolytes at 20 °C. Figure 4b shows that arc was hardly observed in the high frequency part of the AC impedance spectrogram, so a constant phase angle element (CPE) was used instead of the capacitor in the equivalent circuit diagram [39,40]. Figure 4c is the equivalent circuit diagram of the electrolyte that was fitted by Zview software; R_s is the bulk resistance of the electrolyte; R_f is the contact resistance between the gel electrolyte and the platinum electrode. In addition, R_s was fitted by Zview software [41]. The conductivity value was calculated according to the following Equation (1):

$$\sigma = \frac{1}{R_S}\frac{l}{S} \quad (1)$$

where l is the distance between the two platinum electrodes and S is the contact area between the platinum electrode and the electrolyte. In this paper, $l/S = 2\ \mathrm{cm}^{-1}$.

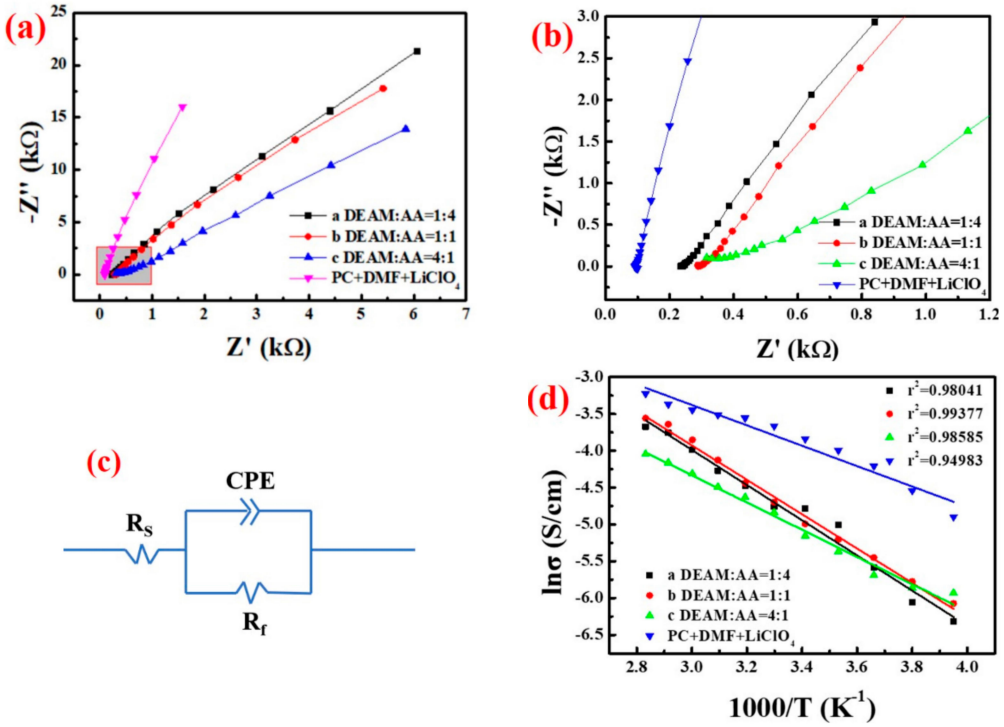

Figure 4. (**a**) AC impedance of PADA gel electrolytes with different volume ratios of DEAM and AA at 20 °C Spectrogram; (**b**) Enlarged view of the rectangular area in (**a**); (**c**) Equivalent circuit diagram of electrolyte fitted by Zview software; (**d**) The ionic conductivity of PADA gel electrolyte with different volume ratios of DEAM and AA changes with temperature.

Figure 4d indicates the relationship between the temperature and the conductivity of a series of PADA gel electrolytes. It shows that the conductivity of gel electrolytes with different ratios increases with the increase of temperature. When the DEAM: AA is 1, the conductivity value of PADA-b gel is higher. The increase in ionic conductivity of the gel electrolyte is because Li^+ in the gel moves faster as the temperature increases. Figure 4d also shows that the ionic conductivities of the PADA gel electrolyte and of the liquid electrolyte are in the same order of magnitude when compared, indicating that the conductivity of gel electrolyte is equivalent to that of liquid electrolyte. The ion conductivity of the PADA-b gel electrolyte is 6.79×10^{-3} S cm^{-1} at 20 °C, which is significantly superior to the PVDF-HFP and PEGDA chemical cross-linked gel polymer electrolyte [42,43] (10^{-5}–10^{-3} S cm^{-1} at room temperature). In addition, the ionic conductivity of PADA-b gel electrolyte is 2.3×10^{-3} S cm^{-1} at −20 °C, indicating that PADA-b gel electrolyte still has a high conductivity at lower temperatures, which extends the temperature range of ECD working normally. This shows that PADA-b gel electrolyte can quickly transport Li^+ when used as an ion-transport layer in electrochromic devices.

We established a relationship between the ionic conductivity and the temperature of the gel electrolyte according to the Arrhenius Equation (2) [41]:

$$\sigma = Aexp\left(\frac{-E_a}{KT}\right) \quad (2)$$

where σ is the ionic conductivity, A is the frequency factor, E_a is the apparent activation energy, K is the rate constant and T is the thermodynamic temperature. Figure 4d shows that the ionic conductivity of a series of PADA gel electrolytes increases with the increase of temperature, indicating that the conduction behavior of the PADA gel electrolyte follows the Arrhenius equation. It is a fact that polymer chains are easier to move at high temperatures, which makes Li^+ transport easier. This shows that the migration movement of Li^+ wrapped

in polymer electrolyte is controlled by temperature. Therefore, the conductive behavior of PADA gel electrolyte is similar to liquid electrolyte.

3.2. Cyclic Stability of Electrochromic Devices

Figure 5a shows the repeated coloring and bleaching process of ECD (WO_3-600) during 150 cycles. When the ECD (WO_3-600) shown in Figure 5b was cycled for the first 11 times, itscolored reflectivity increased, starting from the 12th time initially; the R_c of the electrochromic device remained at about 18.67%; and the R_b remained unchanged at about 14.62%. After 150 bleach/coloring cycles, the R_c and R_b of the electrochromic device were 18.77% and 13.90%, respectively, which indicates that ECD(WO_3-600) has good cycle stability at least for 150 cycles, and that this device retained 95% of its initial performance. This is because the stability performance of electrochromic devices is mainly affected by the stability of the gel electrolyte and the discoloration stability of WO_3.

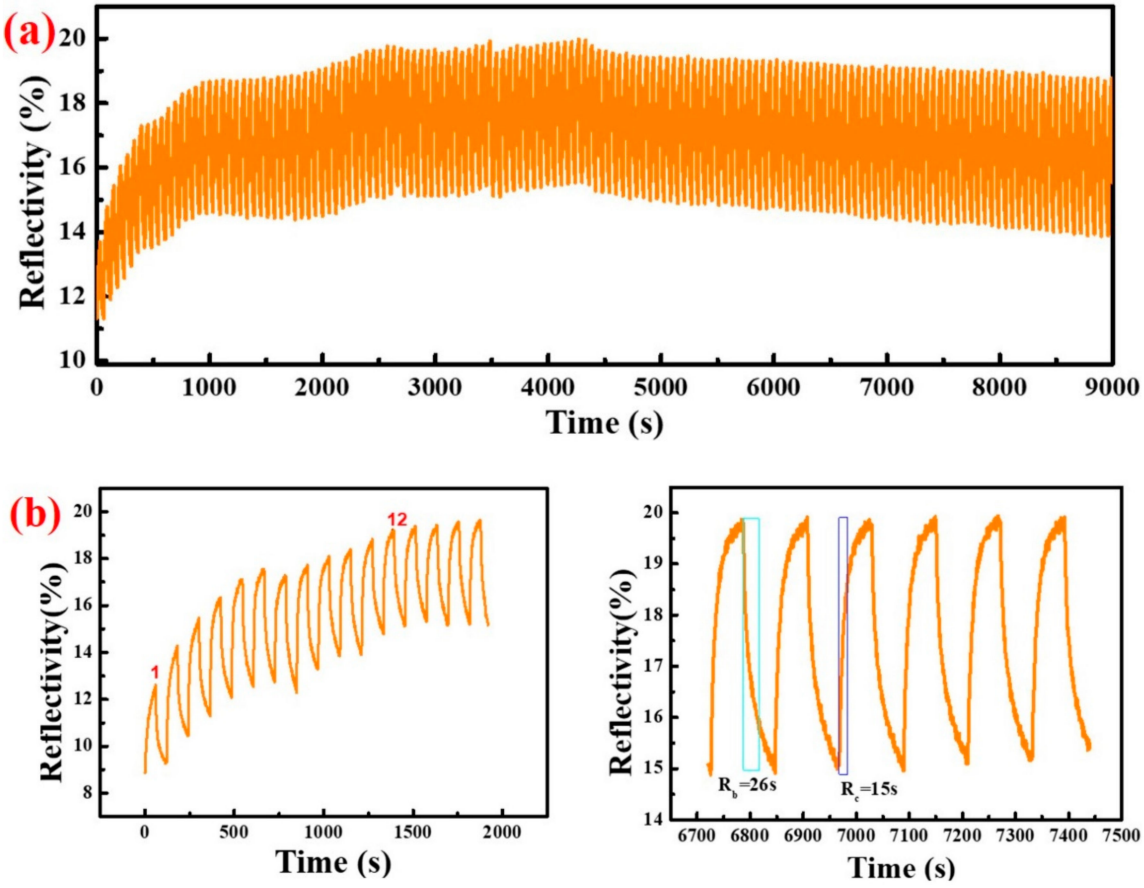

Figure 5. (**a**) The reflectance of the electrochromic device with WO_3 at 700 nm for 150 cycles, applied voltage: ±3.0 V, time: 60 s; (**b**) Shows that the partial enlargement of (**a**): the left picture is 1–16th cycles, and the right picture is 56–62th cycles.

As shown in Figure 6a, when the applied voltage is lower than 3 V, the current through the PADA gel electrolyte is basically stable, which indicates that the gel electrolyte can maintain electrochemical stability at a voltage of 3 V. When the applied voltage is greater than 3 V, the current of the gel electrolyte increases with the increase of the voltage. When the applied voltage reaches 3.4 V, the passing current has increased dramatically, which means that the gel electrolyte begins to decompose at that point, so the electrochemical window of the gel electrolyte is 3.4 V. Figure 6b is the chronocurrent curve of the electrochromic device after sealing the gel electrolyte in the electrochromic device under the voltage condition of ±3 V. This indicates that the current through the electrochromic device is stable in

the coloring/fading state, which also confirms PADA-b gel can maintain electrochemical stability under 3 V voltage, and that the corresponding electrochromic device has better stability performance.

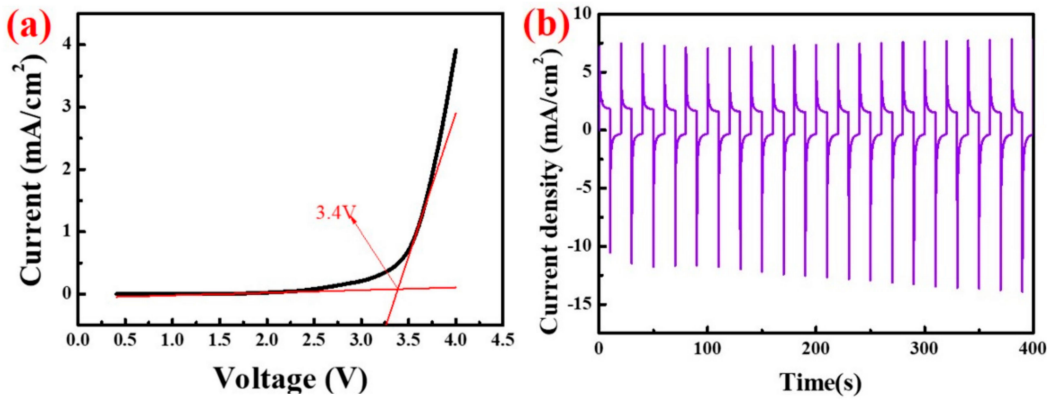

Figure 6. (**a**) Linear sweep volt-ampere curve of PADA-b gel electrolyte; (**b**) Chronoamperometry curve of the ECD (WO_3-600) at a voltage of ±3.0 V.

As mentioned previously, crystalline WO_3 was prepared and applied to electrochromic devices (Figure 1). Tungsten oxide foil was prepared by changing the calcination temperature and controlling other reaction conditions under the same conditions, to explore tungsten oxides with different crystallinity on the electrochromic device. The surface structure of tungsten foil and tungsten oxide foil prepared at different calcination temperatures was analyzed by XRD test (Figure 7a). Figure 7a shows that pure tungsten foil has a long sharp peak at the diffraction angle of 58.1°, and that the other peaks are hardly discovered. WO_3-400 also has a small peak at the diffraction angle of 75.4°, indicating that the surface of the tungsten foil has been oxidized. These two peaks match the characteristic peaks in the hexagonal phase of WO_3 (JCPDS NO.33-1387). Compared with WO_3-400, WO_3-500 has a short and broad peak at a diffraction angle of 23.6°, which is consistent with the characteristic peak in WO_3 tetragonal phase (JCPDS NO.05-0388). It is difficult to observe at a diffraction angle of 75.4° in the XRD diagram of WO_3-600, that the diffraction angle is 23.6° long spikes, and there is a small peak in the diffraction angle of 48.1°, indicating that the sample has a monoclinic phase (JCPDS NO.43-1035) [44–46].

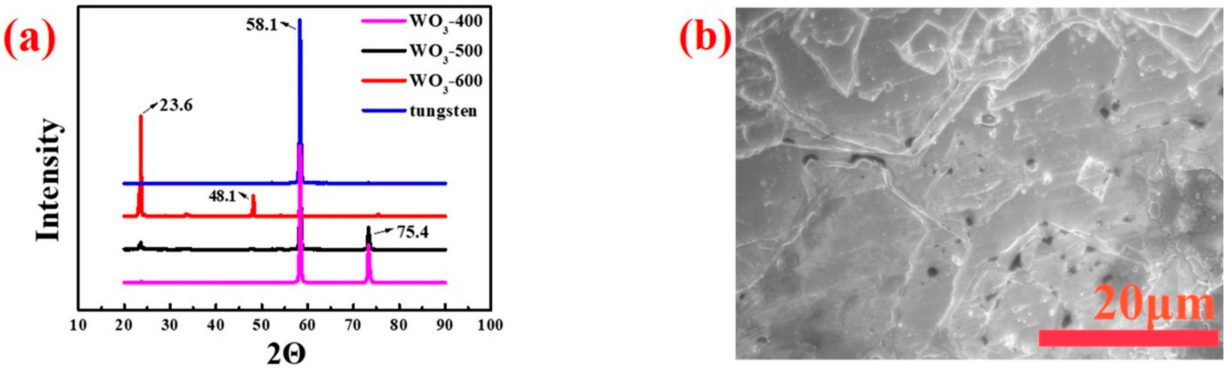

Figure 7. (**a**) XRD images of tungsten foil and tungsten oxide foil (WO_3-X) calcined at different temperatures; (**b**) SEM images of tungsten foil.

Figure 7b and Table 2 show SEM and EDS tests for tungsten foil and tungsten oxide foil, respectively. The results of EDS analysis show that the W/O atomic ratio is close to 1:3, indicating that high-temperature calcined tungsten foil contains WO_3 and basically conforms to the stoichiometric ratio. Figure 7b shows that the surface of the tungsten

foil has a micropore structure, and that the surface of the tungsten oxide foil has many microcracks, which provide a place for Li^+ to be embedded/extracted. As shown in Figure 8a,d,g, the morphology of tungsten oxide foil prepared at different calcination temperatures is analogous. According to the atomic force microscope (AFM) inspections of W and WO_3 surface morphologies in Figure 9, the micropore structure of tungsten oxide foil photographed by SEM is further confirmed. The possibility of different performance of electrochromic devices may reduce due to morphological differences. Therefore, the crystallinity of tungsten oxide may have an effect on the stability performance of the electrochromic device.

Table 2. Element content of W and O in EDS spectrum.

	Element	Tungsten	WO_3-400	WO_3-500	WO_3-600
Weight%	O	0	16.69	21.21	31.32
	W	100	83.31	78.79	68.68
Atomic%	O	0	69.71	75.57	83.98
	W	100	30.29	24.43	16.02

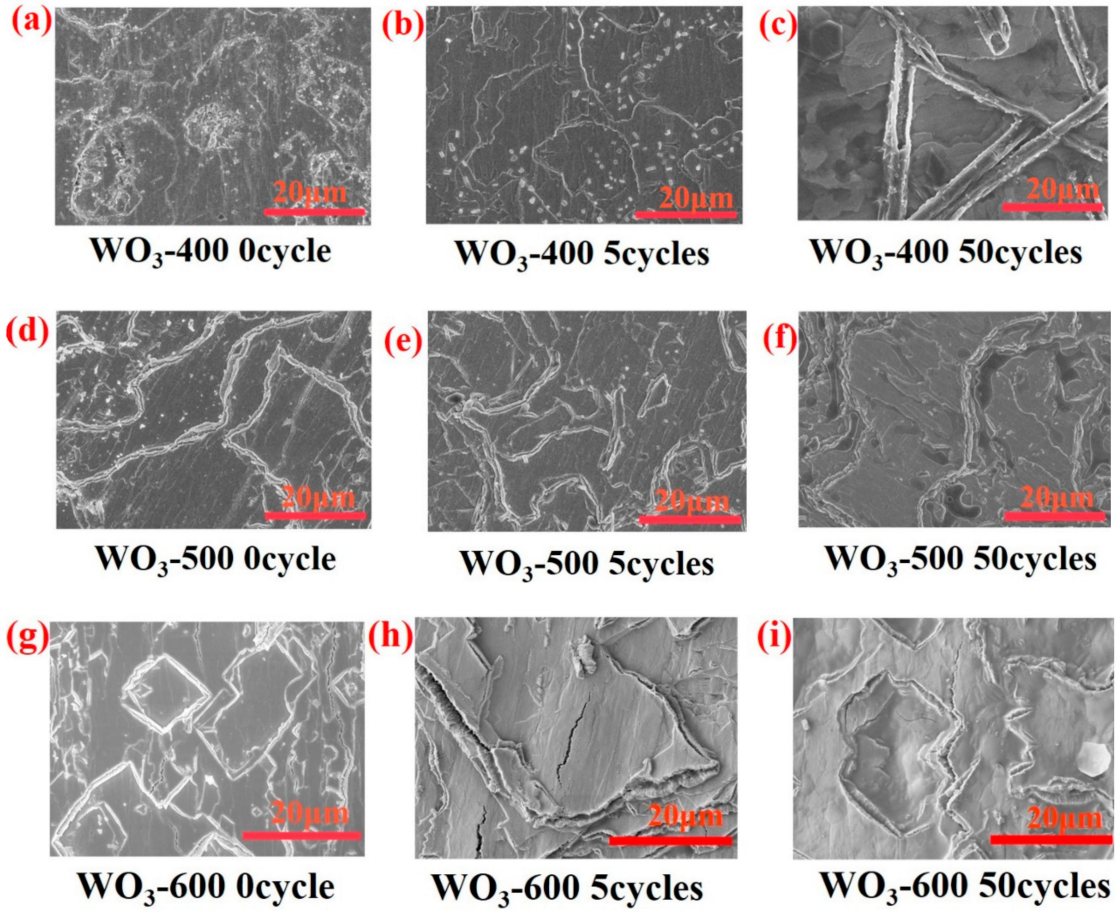

Figure 8. SEM images of WO_3-X (X = 400, 500, 600). (**a**) ECD(WO_3-400) after 0 cycle; (**b**) ECD(WO_3-400) after 5 cycles; (**c**) ECD(WO_3-400) after 50 cycles; (**d**) ECD(WO_3-500) after 0 cycle; (**e**) ECD(WO_3-500) after 5 cycles; (**f**) ECD(WO_3-500) after 50 cycles; (**g**) ECD(WO_3-600) after 0 cycle; (**h**) ECD(WO_3-600) after 5 cycles; (**i**) ECD(WO_3-600) after 50 cycles.

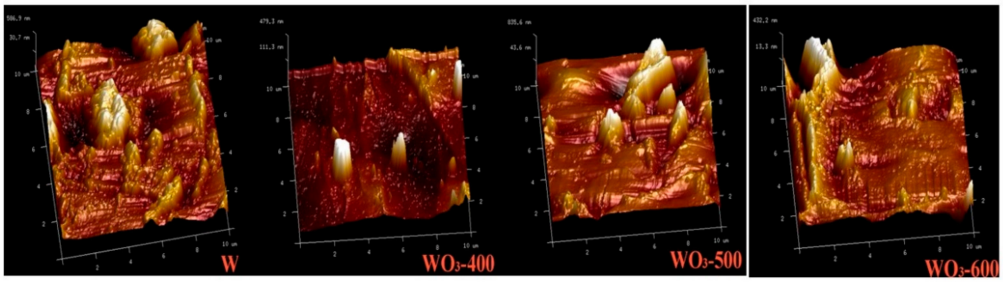

Figure 9. AFM images of W and WO_3-X (X = 400, 500, 600).

Figure 10 indicates that ECD (WO_3-600) has good stability performance after 50 cycles compared to ECD (WO_3-400) and ECD (WO_3-500). The symmetry of the crystal structure of WO_3 increases continuously from monoclinic to tetragonal to hexagonal crystal phase; the corresponding crystal structure becomes more and more stable [47,48]. In this paper, the structure of WO_3-400 and WO_3-500 are more stable compared to WO_3-600, which is not conducive to discoloration; the rate of insertion/extraction of Li^+ in the WO_3 layer becomes slower. Therefore, WO_3-600 has optimum charge transmission performance with the PADA gel polymer electrolyte. It is more suitable as an electrochromic layer, which is consistent with Figure 5b. Figure 5b shows that under the condition of a fixed wavelength, the maximum reflectance of ECD (WO_3-600) coloring continuously increases with the number of cycles. This is because the internal microcracks of WO_3-600 are wider at the beginning (Figure 8g), Li^+ insertion/extraction is easier, and WO_3-600 discoloration speed is fast. As the number of cycles increases to 12, the internal-microcracks-width of the tungsten oxide film is substantially stable, and the coloring/bleaching speed of the tungsten oxide film also becomes stable. The cycle stability of ECD (WO_3-600) can reach at least 150 times, which indicates that the electrochromic device has better stability.

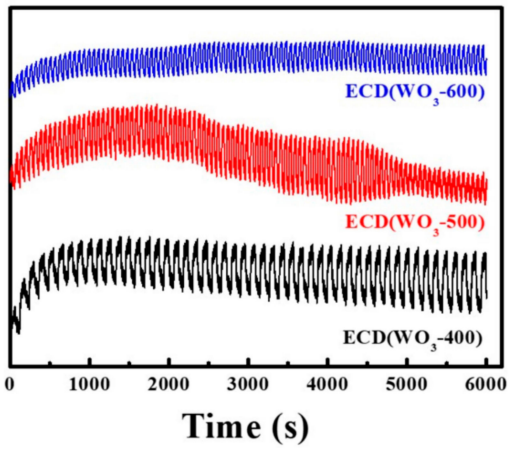

Figure 10. Circulating map of tungsten oxide foil prepared at different calcination temperatures for electrochromic devices, applied voltage: ±3.0 V; WO_3-400 cycle time is 120 s; WO_3-500 and WO_3-600 cycle time are 60 s.

4. Conclusions

In this study, we developed a novel EC device, with an architecture of copper conductive adhesive/tungsten oxide foil/gel electrolyte/nickel foil/transparent PET film, which has no need to use an expensive TCO layer. The influences on phase and micro-structure of high-temperature calcined WO_3 from tungsten foils on the charge-carrier transporting properties in the EC device were investigated. The PADA gel electrolyte had a transmittance of 99.12% at 700 nm, electrical conductivity of 2.3×10^{-3} S cm^{-1} at −20 °C, 6.79×10^{-3} S cm^{-1} at 20 °C, and an electrochemical stability window of 3.4 V. A monoclinic phase crystalline structure was found to be more suitable to this PADA electrolyte. The EC

device with a yellowish-brown (color)/navy blue (bleached) state demonstrated a coloring time of 15 s and a bleaching time of 26 s. In addition, after 150 bleach/coloring cycles, this device retained 95% of its initial performance.

Author Contributions: Conceptualization, W.C. and Y.P.; methodology, G.Z.; validation, G.Z. and S.L.; investigation, M.C., Y.Y.; writing—original draft preparation, W.C. and G.Z.; writing—review and editing, Y.P.; supervision, L.W. All authors have read and agreed to the published version of the manuscript.

Funding: This research received no external funding.

Institutional Review Board Statement: Not applicable.

Informed Consent Statement: Not applicable.

Data Availability Statement: The data presented in this study are available on request from the corresponding author.

Acknowledgments: This work was supported by the National Natural Science Foundation of China (U20A20245, U21A2017).

Conflicts of Interest: There are no conflict of interest to declare.

References

1. Zhang, W.; Li, H.Z.; Yu, W.W.; Elezzabi, A.Y. Transparent inorganic multicolour displays enabled by zinc-based electrochromic devices. *Light Sci. Appl.* **2020**, *9*, 121–132. [CrossRef] [PubMed]
2. Xiao, S.X.; Zhang, Y.J.; Ma, L.; Zhao, S.; Wu, N.; Xiao, D. Easy-to-make sulfonatoalkyl viologen/sodium carboxymethylcellulose hydrogel-based electrochromic devices with high coloration efficiency, fast response and excellent cycling stability. *Dye. Pigment* **2020**, *174*, 108055. [CrossRef]
3. Wu, W.; Wang, M.; Ma, J.M.; Cao, Y.L.; Deng, Y.H. Electrochromic Metal Oxides: Recent Progress and Prospect. *Adv. Electron. Mater.* **2018**, *4*, 1800185–1800204. [CrossRef]
4. Yang, P.H.; Sun, P.; Mai, W.J. Electrochromic energy storage devices. *Mater. Today* **2016**, *19*, 394–402. [CrossRef]
5. Granqvist, C.G. Electrochromics for smart windows: Oxide-based thin films and devices. *Thin Solid Film.* **2014**, *564*, 1–38. [CrossRef]
6. Granqvist, C.G. Oxide electrochromics: An introduction to devices and materials. *Sol. Energy Mater. Sol. Cells* **2012**, *99*, 1–13. [CrossRef]
7. Yu, H.; Shao, S.; Yan, L.; Meng, H.; He, Y.; Yao, C.; Xu, P.; Zhang, X.; Hu, W.; Huang, W. Side-chain engineering of green color electrochromic polymer materials: Toward adaptive camouflage application. *J. Mater. Chem. C* **2016**, *4*, 2269–2273. [CrossRef]
8. Niu, J.L.; Wang, Y.; Zou, X.L.; Tan, Y.; Jia, C.Y.; Weng, X.L.; Deng, L.G. Infrared electrochromic materials, devices and applications. *Appl. Mater. Today* **2021**, *24*, 101073. [CrossRef]
9. Wang, Z.; Wang, X.Y.; Cong, S.; Chen, J.; Sun, H.Z.; Chen, Z.G.; Song, G.; Geng, F.X.; Chen, Q.; Zhao, Z.G. Towards full-colour tunability of inorganic electrochromic devices using ultracompact fabry-perot nanocavities. *Nat. Commun.* **2020**, *11*, 302. [CrossRef]
10. Shenouda, S.S.; AlAbdulaa, T.H.; Zahran, H.Y.; Yahia, I.S. Synthesis, structure identification and linear/nonlinear optics of hydrothermally grown WO_3 nanostructured thin film/FTO: Novel approach. *Ceram. Int.* **2021**, *11*, 311. [CrossRef]
11. Lakshmi, M.; Avani, A.V.; Kathirvel, P.; Marnadu, R.; Packiaraj, R.; Joshua, J.R.; Nallamuthu, N.; Shkir, M.; Saravanakumar, S. Investigation on structural, morphological and electrochemical properties of Mn doped WO_3 nanoparticles synthesized by co-precipitation method for supercapacitor applications. *J. Alloys Compd.* **2021**, *882*, 160670. [CrossRef]
12. Shi, Y.Z.; Liu, Q.Y.; Hong, R.J.; Tao, C.X.; Wang, Q.; Lin, H.; Han, Z.X.; Zhang, D.W. SERS-active WO_3-x thin films with tunable surface plasmon resonance induced by defects from thermal treatment. *Spectrochim. Acta Part A Mol. Biomol. Spectrosc.* **2021**, *268*, 120686. [CrossRef]
13. Muñoz-Bolaños, J.D.; Rodríguez-Páez, J.E. WO_3 mono-nanocrystals: Synthesis, characterization and evaluation of their electrical behavior in oxygen and acetone atmospheres. *Mater. Sci. Eng. B* **2021**, *274*, 115472. [CrossRef]
14. Oscar, H.-A.; Rafael, A.; Aníbal, S. DFT+U study of the electronic structure changes of WO_3 monoclinic and hexagonal surfaces upon Cu, Ag, and Au adsorption. Applications for CO adsorption. *Surf. Sci.* **2021**, *714*, 121907. [CrossRef]
15. Lyu, H.L. Triple layer tungsten trioxide, graphene, and polyaniline composite films for combined energy storage and electrochromic applications. *Polymers* **2019**, *12*, 49. [CrossRef]
16. Granqvist, C.G. Electrochromic tungsten oxide films: Review of progress 1993–1998. *Sol. Energy Mater. Sol. Cells* **2000**, *60*, 201–262. [CrossRef]
17. Granqvist, C.G.; Green, S.; Niklasson, G.A.; Mlyuka, N.R.; von Kræmer, S.; Georén, P. Advances in chromogenic materials and devices. *Thin Solid Film.* **2010**, *518*, 3046–3053. [CrossRef]

18. Perfecto, T.M.; Zito, C.A.; Volanti, D.P. Design of nanostructured $WO_3 \cdot 0.33\ H_2O$ via combination of ultrasonic spray nozzle and microwave-assisted hydrothermal methods for enhancing isopropanol gas sensing at room temperature. *CrystEngComm* **2017**, *19*, 2733–2738. [CrossRef]
19. Chang, X.T.; Hu, R.R.; Sun, S.B.; Liu, J.R.; Lei, Y.H.; Liu, T.; Dong, L.H.; Yin, Y.S. Sunlight-charged electrochromic battery based on hybrid film of tungsten oxide and polyaniline. *Appl. Surf. Sci.* **2018**, *441*, 105–112. [CrossRef]
20. Ahmadian, H.; Tehrani, F.S.; Aliannezhadi, M. Hydrothermal synthesis and characterization of WO_3 nanostructures: Effects of capping agent and pH. *Mater. Res. Express* **2019**, *6*, 105024. [CrossRef]
21. Abbaspoor, M.; Aliannezhadi, M.; Tehrani, F.S. Effect of solution pH on as-synthesized and calcined WO_3 nanoparticles synthesized using sol-gel method. *Opt. Mater.* **2021**, *121*, 111552. [CrossRef]
22. Pooyodying, P.; Son, Y.-H.; Sung, Y.-M.; Ok, J.-W. The effect of sputtering Ar gas pressure on optical and electrical properties of flexible ECD device with WO_3 electrode deposited by RF magnetron sputtering on ITO/PET substrate. *Opt. Mater.* **2022**, *123*, 111829. [CrossRef]
23. Sharma, A.; Saini, A.K.; Kumar, N.; Tejwan, N.; Singh, T.A.; Thakur, V.K.; Das, J. Methods of preparation of metal-doped and hybrid tungsten oxide nanoparticles for anticancer, antibacterial, and biosensing applications. *Surf. Interfaces* **2022**, *28*, 101641. [CrossRef]
24. Wei, S.H.; Zhao, J.H.; Hu, B.X.; Wu, K.Q.; Du, W.M.; Zhou, M.H. Hydrothermal synthesis and gas sensing properties of hexagonal and orthorhombic WO_3 nanostructures. *Ceram. Int.* **2017**, *43*, 2579–2585. [CrossRef]
25. Han, X.P.; Amrane, N.; Qamhieh, N.; Benkraouda, M. Enhanced optoelectronic functionality of N + H codoped monoclinic WO_3: A hybrid functional study. *Chem. Phys.* **2021**, *549*, 111283. [CrossRef]
26. Hajiahmadi, Z.; Azar, Y.T. Computational study of h-WO_3 surfaces as a semiconductor in water-splitting application. *Surf. Interfaces* **2021**, *28*, 101695. [CrossRef]
27. Feng, M.C.; Liu, Y.N.; Zhao, Z.Y.; Huang, H.W.; Peng, Z.J. The preparation of Fe doped triclinic-hexagonal phase heterojunction WO_3 film and its enhanced photocatalytic reduction of Cr (VI). *Mater. Res. Bull.* **2019**, *109*, 168–174. [CrossRef]
28. Jamali, M.; Tehrani, F.S. Effect of synthesis route on the structural and morphological properties of WO_3 nanostructures. *Mater. Sci. Semicond. Process.* **2020**, *107*, 104829. [CrossRef]
29. Jamali, M.; Tehrani, F.S. Thermally stable WO_3 nanostructure synthesized by hydrothermal method without using surfactant. *Mater. Sci. Eng. B* **2021**, *270*, 115221. [CrossRef]
30. Jayatissa, A.H.; Dadi, A.; Aoki, T. Nanocrystalline WO_3 films prepared by two-step annealing. *Appl. Surf. Sci.* **2005**, *244*, 453–457. [CrossRef]
31. Li, T.Y.; Li, X.L.; Bae, J.Y.; Kim, S.H.; Moon, H.C. Non-volatile, Li-doped ion gel electrolytes for flexible WO_3-based electrochromic devices. *Mater. Des.* **2019**, *162*, 45–51. [CrossRef]
32. Chen, W.Y.; Zhu, C.Z.; Guo, L.; Yan, M.Y.; Wu, L.L.; Zhu, B.; Qi, C.J.; Liu, S.Y.; Zhang, H.; Peng, Y. A novel ionically crosslinked gel polymer electrolyte as iontransport layer for high performance electrochromic devices. *J. Mater. Chem. C* **2019**, *7*, 3744–3750. [CrossRef]
33. Chen, P.; Liang, X.P.; Wang, J.; Zhang, D.; Yang, S.M.; Wu, W.S.; Zhang, W.; Fan, X.W.; Zhang, D.Q. PEO/PVDF-based gel polymer electrolyte by incorporating nano-TiO_2 for electrochromic glass. *J. Sol-Gel Sci. Technol.* **2016**, *81*, 850–858. [CrossRef]
34. Li, F.-W.; Yen, T.-C.; Liou, G.-S. Synthesis of high-performance electrochromic material for facile fabrication of truly black electrochromic devices. *Electrochim. Acta* **2021**, *367*, 137474. [CrossRef]
35. Ramadan, R.; Kamal, H.; Hashem, H.M.; Abdel, H.K. Gelatin-based solid electrolyte releasing Li^+ for smart window applications. *Sol. Energy Mater. Sol. Cells* **2014**, *127*, 147–156. [CrossRef]
36. Dulgerbaki, C.; Oksuz, A.U. Poly (3-methylthiophene)/Tungsten oxide hybrid materials for highly efficient electrochromic devices. *Opt. Mater.* **2021**, *119*, 111354. [CrossRef]
37. Xiang, S.F.; Chen, S.S.; Yao, M.T.; Zheng, F.; Lu, Q.H. Strain sensor based on a flexible polyimide ionogel for application in high-and low-temperature environments. *J. Mater. Chem. C* **2019**, *7*, 9625–9632. [CrossRef]
38. Hsiao, L.-Y.; Chang, T.-H.; Lu, H.-C.; Wang, Y.-C.; Lu, Y.-A.; Ho, K.-C.; Higuchi, M. A panchromatic electrochromic device composed of Ru (II)/Fe (II)-based heterometallo-supramolecular polymer. *J. Mater. Chem. C* **2019**, *7*, 7554–7562. [CrossRef]
39. Kumar, G.G.; Munichandraiah, N. A gel polymer electrolyte of magnesium triflate. *Solid State Ion.* **2000**, *128*, 203–210. [CrossRef]
40. Brug, G.J.; van den Eeden, A.L.G.; Sluyters-Rehbach, M.; Sluyters, J.H. The analysis of electrode impedances complicated by the presence of a constant phase element. *J. Electroanal. Chem. Interfacial Electrochem.* **1984**, *176*, 275–295. [CrossRef]
41. Chen, W.; Liu, S.; Guo, L.; Zhang, G.; Zhang, H.; Cao, M.; Wu, L.; Xiang, T.; Peng, Y. A Self-Healing Ionic Liquid-Based Ionically Cross-Linked Gel Polymer Electrolyte for Electrochromic Devices. *Polymers* **2021**, *13*, 742. [CrossRef]
42. Zhao, Y.; Liu, H.B.; Meng, X.H.; Liu, A.M.; Chen, Y.; Ma, T.L. A cross-linked tin oxide/polymer composite gel electrolyte with adjustable porosity for enhanced sodium ion batteries. *Chem. Eng. J.* **2021**, *431*, 133922. [CrossRef]
43. Liu, M.; Zhang, S.T.; Li, G.Q.; Wang, C.; Li, B.; Li, M.; Wang, Y.; Ming, H.; Wen, Y.H.; Qiu, J.Y.; et al. A cross-linked gel polymer electrolyte employing cellulose acetate matrix and layered boron nitride filler prepared via in situ thermal polymerization. *J. Power Sources* **2021**, *484*, 229235. [CrossRef]
44. Petruleviciene, M.; Juodkazyte, J.; Parvin, M.; Tereshchenko, A.; Ramanavicius, S.; Karpicz, R.; Samukaite-Bubniene, U.; Ramanavicius, A. Tuning the Photo-Luminescence Properties of WO_3 Layers by the Adjustment of Layer Formation Conditions. *Materials* **2020**, *13*, 2814. [CrossRef]

45. Ram, J.; Singh, R.G.; Gupta, R.; Kumar, V.; Singh, F.; Kumar, R. Effect of annealing on the surface morphology, optical and and structural properties of nanodimensional tungsten oxide prepared by coprecipitation technique. *J. Electron. Mater.* **2019**, *48*, 1174–1183. [CrossRef]
46. Shendage, S.S.; Patil, V.L.; Vanalakar, S.A.; Harale, N.S.; Bhosale, J.L.; Kim, J.H.; Payil, P.S. Sensitive and selective NO_2 gas sensor based on WO_3 nanoplates. *Sens. Actuators B Chem.* **2017**, *240*, 426–433. [CrossRef]
47. Balaji, S.; Djaoued, Y.; Albert, A.S.; Brüning, R.; Beaudoin, N.; Robichaud, J. Porous orthorhombic tungsten oxide thin films: Synthesis, characterization, and application in electrochromic and photochromic devices. *J. Mater. Chem.* **2011**, *21*, 3940–3948. [CrossRef]
48. Afify, H.H.; Hassan, S.A.; Obaida, M.; Moussa, I.; Abouelsayed, A. Preparation, characterization, and optical spectroscopic studies of nanocrystalline tungsten oxide WO_3. *Opt. Laser Technol.* **2019**, *111*, 604–611. [CrossRef]